Inorganica Chimica Acta 415 (2014) 52–60

Contents lists available at ScienceDirect

Inorganica Chimica Acta

journal homepage: www.elsevier.com/locate/ica

# Effects of the π-conjugation length of bipyridyl ligand on the photophysical properties of binuclear organotin(IV) complexes: Synthesis and characterization of dimethyltin(IV) complexes with bipyridyl

Ezzatollah Najafi [a], Mostafa M. Amini [a,*], Mohammad Janghouri [b], Ezeddine Mohajerani [b], Seik Weng Ng [c,d]

[a] Department of Chemistry, Shahid Beheshti University, G.C., Tehran 1983963113, Iran
[b] Laser Research Institute, Shahid Beheshti University, G.C., Tehran 1983963113, Iran
[c] Department of Chemistry, University of Malaya, 50603 Kuala Lumpur, Malaysia
[d] Department of Chemistry, Faculty of Science, King Abdulaziz University, PO Box 820203, Jaddah, Saudi Arabia

ARTICLE INFO

*Article history:*
Received 7 November 2013
Received in revised form 5 February 2014
Accepted 22 February 2014
Available online 11 March 2014

*Keywords:*
Tin(IV) complex
Crystal structure
Photoluminescence
Electroluminescence
OLED

ABSTRACT

The dimethyltin(IV) complexes of rigid bipyridyl-based ligands, 4,4′-bipyridine (4,4′-bipy) and 1,4-bis(4-pyridyl)-2,3-diaza-1,3-butadiene (4-bpdb), were prepared and characterized by $^{1}H$, $^{13}C$ and $^{119}Sn$ NMR, IR, and UV spectroscopies, single-crystal X-ray diffraction and elemental analysis. The prepared complexes were used as green and yellow-orange electroluminescence dopant materials to fabricate organic light-emitting diodes (OLEDs) with a general configuration of ITO/PEDOT:PSS(90 nm)/PVK:PBD:tin-complexes (80 nm)/Al(200 nm). The effects of long and rigid bipyridyl-based ligands on the electroluminescence properties of the complexes were investigated. The maximum emission peaks showed that a good correlation exists between the π-conjugation length of bipyridyl ligands and emission wavelength. Replacing 4-bpdb with the long π-conjugation length, 4,4′-bipy, resulted in red shifts in both absorption and fluorescence spectra and moderately enhanced the photoluminescence intensity and the fluorescence quantum yield. Furthermore, complex of dimethyltin(IV) with 4-bpdb ligand was doped into a PVK:PBD blend as the host in two different concentrations. It was found that the high concentration of dopant caused a trap effect in the current voltage and led to a self-quenching of emission and reduced the efficiency of the device.



## 1. Introduction

Organic electroluminescent (EL) devices have recently received a considerable amount of attention since they can be utilized to produce emissions of all colors in accordance with a wide selection of organic emitting materials [1–5]. One of their possible applications is in the fabrication of large-area light-emitting displays, which are difficult to achieve using inorganic light-emitting cells. Many attempts have been made to design and synthesize a wide variety of coordination compounds as electronic materials for the fabrication of low-cost OLED devices in convenient processes [6–8]. Choosing a suitable ligand and metal is very important for attaining a well-designed coordination compound with good applicability in the fabrication of OLEDs [9]. A large number of metal complexes of main and transition metal ions have been reported for EL applications. However, little attention has been focused on the EL properties of the group IVA metal complexes, in general, and tin(IV) complexes, in particular [10–13]. The coordination chemistry of tin is very interesting because of its variable valence (divalent and tetravalent) states and structural diversity. Furthermore, tin has a higher work function than the group IIB and IIIA elements due to the higher ionization potential of tin complexes than those of other metal complexes [14,15]. Therefore, the synthesis of tin(IV) complexes containing conjugated ligands (well-known ligands in the field of photonic) should provide a basis for luminescent studies and that could provide an opportunity to utilize them in fabrication of OLED devices. It was found that the EL properties of OLEDs are strongly coupled to the molecular structures of the dopants in the OLED devices [16–19]. To the best of our knowledge, the relationship between the electroluminescent properties of OLEDs and the structure of tin complexes has not been reported. We are interested in learning how the structures of the tin complexes influence the OLED's brightness and in

* Corresponding author. Tel.: +98 21 29903109; fax: +98 21 2243166.
*E-mail address:* m-pouramini@sbu.ac.ir (M.M. Amini).

http://dx.doi.org/10.1016/j.ica.2014.02.032
0020-1693/

evaluating the electroluminescence performance of the tin complex-doped OLEDs devices. In continuation of our interest in the effect of the structures of tin complexes on the electroluminescence (EL) properties of the organic light-emitting diode (OLED), we chose two long-chain rigid bipyridyl-based ligands as primary ligands, 4,4′-bipyridine (4,4′-bipy) and 1,4-bis(4-pyridyl)-2,3-diaza-1,3-butadiene (4-bpdb), and reacted them with dimethyltin(IV) dichloride to prepare two new organotin complexes. Furthermore, in order to enhance the optical properties of tin complexes, cupferron was used as an auxiliary ligand in complexes. Then, the prepared complexes were utilized as green and yellow-orange EL dopant materials to fabricate OLED devices with a general configuration of ITO/PEDOT:PSS(90 nm)/PVK:PBD:tin-complex (80 nm)/Al(200 nm). Furthermore, we investigated the electronic state energy levels (HOMO/LUMO) of the complexes via cyclic voltammetry measurements, current–voltage curves (I–V), and photoluminescence in solutions. From these data, the relationship between the structures of tin compounds and the performance of the devices was accomplished. A photophysical study of the prepared complexes revealed that the intensity of the fluorescence band of the complex containing the long conjugate rigid ligand (**2**) was higher than the band of the complex with the short conjugate ligand (**1**). In addition, both absorption and emission peaks of the complex **2** red shifted significantly in comparison with those of the complex **1**.

## 2. Experimental

### 2.1. Materials and physical measurements

Exception for the 1,4-bis(4-pyridyl)-2,3-diaza-1,3-butadiene (4-bpdb) ligand which was prepared according to the literature procedures [20], all other reagents were purchased from Merck and used without further purification. All solvents were dried and distilled under a nitrogen atmosphere prior to use, according to a standard procedure [21]. Melting point was obtained with an Electrothermal 9200 melting point apparatus and is not corrected. Infrared spectra from 250 to 4000 $cm^{-1}$ were recorded on a Shimadzu 470 FT-IR instrument, using KBr pellets. NMR spectra were recorded at room temperature in DMSO on a Bruker AVANCE 300-MHz operating at 300.3 MHz. Elemental analyses was performed with a Thermo Finnigan Flash-1112EA microanalyzer. The thermal analysis (TGA-DTA) was carried out on a Bahr STA-503 instrument under air atmosphere. The thickness of the samples was measured using a DekTak 8000 profilometer. The electroluminescence and photoluminescence spectra of fabricated OLEDs were obtained on a HR4000 Oceanoptic and USB2000 spectrometers, respectively. The current–voltage and luminance were checked by Keithley 2400 and Minolta Luminance meter LS110, respectively. Quantum yields were determined using quinine sulfate in 1.0 N $H_2SO_4$ ($\phi = 0.54$). UV–Vis spectra were recorded on a Shimadzu 2100 spectrometer. The ionization potential of tin complexes was determined by a photoemission apparatus (Riken Keiki AC).

### 2.2. X-ray crystallography

Single-crystal X-ray diffraction data were collected on a Bruker SMART APEX with graphite monochromated Mo-Kα radiation at 100 K using APEX2 software [22]. For [μ-(4,4′-bipy){$Me_2$-Sn(cupf)$_2$}$_2$]·EtOH complex (**1**), a yellow prismatic crystal with a dimension of 0.25 × 0.25 × 0.25 mm and for [μ-(4-bpdb){$Me_2$-Sn(cupf)$_2$}$_2$]·MeOH complex (**2**), a yellow block crystal with a dimension of 0.30 × 0.25 × 0.20 mm were mounted on a glass fiber and used for data collection. Cell constants and an orientation matrix for the data collection were obtained by least-squares refinement of diffraction data from 4335 for **1** and 4882 for **2** unique reflections. Data were collected to a maximum $2\theta$ value of 27.6° for **1** and 27.56° for **2**. The numerical absorption coefficient, $\mu$, for Mo Kα radiation is 1.243 $mm^{-1}$ for **1** and 1.158 $mm^{-1}$ for **2**. A numerical absorption correction was applied using SADABS software [23]. The data were corrected for Lorentz and Polarizing effects. The structures were solved by direct method and subsequent difference Fourier map and then refined on $F^2$ by a full-matrix least-squares procedure using anisotropic displacement parameters methods [24]. Subsequent refinement then converged with R factors, and parameters errors significantly better than for all attempts to model the solvent disorder. All refinements were performed using the SHELXL97 crystallographic software package [25].

### 2.3. Synthesis of complexes

#### 2.3.1. Preparation of [μ-(4,4′-bipy){$Me_2Sn(cupf)_2$}$_2$]·EtOH (**1**)

All manipulations were performed under an atmosphere of dry nitrogen using standard Schlenk line technique. For preparation of title complex, a solution of 4,4′-bipyridine (0.16 g, 1.0 mmol) in ethanol (20 mL) was added to a solution of dimethyltin(IV) dichloride (0.22 g, 1.0 mmol) in ethanol (10 mL). A white precipitation was rapidly formed. The mixture was stirred for 10 min at room temperature and then $NH_4$[PhN(O)NO] salt (0.31 g, 2.0 mmol) was added to the reactor. The $NH_4Cl$ promptly precipitated and the resulting yellow solution was stirred for one hour at room temperature. The precipitate was filtered off and the mother liquor was left to evaporate slowly at room temperature. After one week, yellow crystals of title complex were isolated (yield 75%; m.p. 130–132 °C). *Anal.* Calc. for $C_{40}H_{46}N_{10}O_9Sn_2$: C, 45.83; H, 4.42; N, 13.36. Found: C, 45.79; H, 4.39; N, 13.45%. IR (KBr, $cm^{-1}$): $\nu$(m, O–H), 3480; $\nu$(w, $C_{ph}$–H), 3075; $\nu$(m, C–H), 2920; $\nu$(m, C=C), 1465; $\nu$(m, N–N), 1334; $\nu$(s, N=O), 1210; $\nu$(s, ONNO), 1055; $\nu$(m, Sn–C), 520; $\nu$(Sn–N), 461; $\nu$(Sn–O), 400. $^1$H NMR (DMSO, ppm): 0.61 (6H, s, Sn-$CH_3$, $^2J^{117/119}$Sn-H = 116 Hz), 7.38–8.74 (14H, m, $C_6H_5$ and $C_5H_5N$). $^{13}$C NMR (DMSO-$d_6$, ppm): 9.3 ($CH_3$, $^1J^{117/119}$Sn–$^{13}$C = 1097), 118.3 (C4, C8, C10, C14), 120.8 (C16, C18), 124.5 (C5, C7, C11, C13), 129.3 (C6, C12), 142.2 (C17), 148.4 (C15, C19), 151.2 (C3, C9). $^{119}$Sn NMR (DMSO-$d_6$, ppm): −382.5.

#### 2.3.2. Preparation of [μ-(4-bpdb){$Me_2Sn(cupf)_2$}$_2$]·MeOH (**2**)

Compound **2** was synthesized in the same way as compound **1** using 4-bpdb in instead of 4,4′-bipyridine (yield 82%; m.p. 178–180 °C). *Anal.* Calc. for $C_{41}H_{46}N_{12}O_9Sn_2$: C, 45.25; H, 4.26; N, 15.44. Found: C, 45.48; H, 4.01; N, 15.91%. IR (KBr, $cm^{-1}$): $\nu$(m, O–H), 3370; $\nu$(w, $C_{ph}$–H), 3065; $\nu$(m, C–H), 2906; $\nu$(m, C = C), 14735; $\nu$(m, N–N), 1301; $\nu$(s, N=O), 1228; $\nu$(s, ONNO), 1049; $\nu$(m, Sn–C), 516; $\nu$(Sn–N), 459; $\nu$(Sn–O), 402. $^1$H NMR (DMSO, ppm): 0.48 (12H, s, Sn–$CH_3$, $^2J^{117/119}$Sn–H = 116 Hz), 7.79–8.75 (30H, m, $C_6H_5$ and $C_5H_5N$). $^{13}$C NMR (DMSO, ppm): 8.6 ($CH_3$, $^1J^{117/119}$Sn–$^{13}$C = 1097 Hz), 117.2 (C4, C8, C10, C14), 120.7 (C16, C18), 126.1 (C5, C7, C11, C13), 126.9.3 (C6, C12), 143.1 (C17), 149.1 (C15, C19, C20), 150.1 (C3, C9). $^{119}$Sn NMR (DMSO, ppm): −371.

### 2.4. Fabrication of OLED by utilization of the prepared complexes

Fig. S1 (Electronic Supplementary information; ESI) shows the line drawing structures of the prepared complexes and axillary materials that used for fabrication of OLED device. The structure of the fabricated device is as follows: ITO/PEDOT:PSS(90 nm)/PVK:PBD(80 nm)/Al(200 nm) and ITO/PEDOT:PSS(90 nm)/PVK:PBD:tin complexes (80 nm)/Al(200 nm). The final sample structure is shown in Fig. 1. The first step in the fabrication process was cleaning ITO substrates by detergent, acetone, dichloromethane,

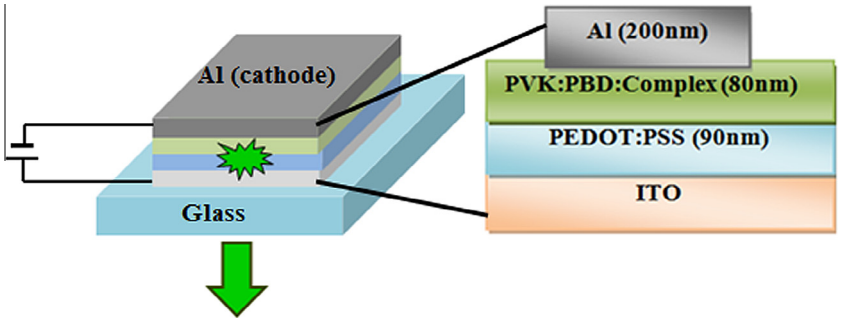


**Fig. 1.** Layer arrangement and layer thickness of the OLED devices.

dichloroethane, ethanol, methanol and deionized water in ultrasonic bath. PEDOT:PSS as a hole-injection layer was then spin coated on a clean ITO substrate at thickness of 90 nm. The coated layer was then baked for one hour at 120 °C to reduce the surface roughness. PVK as a hole-transporting material and PBD as an electron-transporting material were doped with tin complexes. The ratio of tin complex for each type was 10 wt% in PVK:PBD (100:40). PVK, PBD and tin complexes with the ratio of 100:40:10 were blended in DMF and then spin coated and baked at 80 °C for 1 h. Finally, a metallic cathode of Al was deposited on the emissive layer at $8 \times 10^{-5}$ mbar by thermal evaporation. The active area of the prepared samples was $6 \times 6$ mm$^2$.

## 3. Results and discussion

### 3.1. Synthesis

Both complexes were isolated in moderate yields from the reaction of dimethyltin(IV) dichloride, corresponding bipyridyl ligand and cupferron, and were fully characterized by various techniques. These reactions were fast and facile, and their progress was monitored through the appearance of fluorescence colors. The elemental analyses and the IR and NMR spectral data of the **1** and **2** are in accordance with the formulas [μ-(4,4′-bipy){$Me_2Sn(cupf)_2$}$_2$]·EtOH and [μ-(4-bpdb){$Me_2Sn(cupf)_2$}$_2$]·MeOH, respectively. The prepared complexes are stable in air and soluble in chloroform and can be accumulated at room temperature for an indistinct period of time. The good stability of the complexes is probably associated with the overall molecule, which is linked together by covalent Sn-O and Sn-N bonds that provide adequate thermodynamic and kinetic stability for existence in the solid state.

### 3.2. General characterization

In the IR spectra of the prepared complexes, the absence of a stretching vibration at the 3160 cm$^{-1}$ (associated with the ammonium salt of the cupferron ligand) clearly indicates the formation of the Sn–O bonds. The stretching vibration band of Sn–O is important data and can be related to the bonding mode of the ligand. When the cupferronato anion coordinates to the tin center in the common bidentate chelating mode, the ν(Sn–O) band appears in the 399–406 cm$^{-1}$ range, while, for a bridging coordination pattern, the ν(Sn–O) band appears around 389 cm$^{-1}$ [26]. In **1** and **2**, this band was observed at about 400 cm$^{-1}$. The new band at about 461 cm$^{-1}$ in comparison with the IR spectra of the free bipyridyl ligands was assigned to the Sn–N vibration, and this unambiguously proved the coordination of nitrogen to tin. The presence of a single Sn–C stretching vibration band at about 520 cm$^{-1}$ in the infrared spectra of the complexes indicates that the C–Sn–C bond angle is close to 180°. This is in accordance with the X-ray diffraction results. For the determination of the structural features of **1** and **2** in solution the $^1$H, $^{13}$C and $^{119}$Sn NMR spectra were recorded. The $^1$H NMR spectra of the complexes showed the expected aliphatic and aromatic peaks with the correct integration, and the $^2J^{117/119}$Sn–H coupling constant of 116 Hz for both complexes is consistent with pentagonal bipyramidal geometry about the tin atom. Based on the magnitude of $^2J^{117/119}$Sn-H, the C-Sn-C angle is estimated to be 171° for both compounds. In the $^{13}$C NMR spectra of the compounds, the signals of ligands are shifted only slightly from their position in the spectra of the free donor ligands which can be attributed to the coordination of cupferron and bipyridyl ligands to tin and formation of Sn–N and Sn–O bonds.

### 3.3. Single-crystal X-ray analyses

The molecular structures of **1** and **2** were established with single-crystal X-ray diffraction analysis and results are shown in Figs. 2 and 3 along with the atom numbering schemes. Crystal data and refinement details and selected bond distances and angles for **1** and **2** are listed in Tables 1–3.

Compound **1** crystallized in the monoclinic system in the space group of $P2_{1/n}$. The structure of complex consists of centrosymmetric binuclear [$(CH_3)_2Sn(O_2N_2(C_6H_5)_2]_2$.4,4′-bipy units, which the asymmetric unit contains one independent tin atom. The coordination geometry around the tin atom is distorted pentagonal bipyramidal and the tin hepta-coordinated axially by two tin-bound methyl carbon atoms and equatorially by the $O_4N$ donor set of the cupferronato and the bipy ligands. The sum of the bond angles of O(1)–Sn(1)–O(2), 67.95(5)°; O(1)–Sn(1)–O(4), 74.97(5)°; O(4)–Sn(1)–O(3), 66.92(5)°, O(3)–Sn(1)–N(5) 74.47(6)° and O(2)–Sn(1)–N(5), 75.88(6)° is 360.1°. This shows that the Sn(1), O(1), O(2), O(3), O(4) and N(5) atoms are coplanar. Therefore, the coordination at Sn(1) atom can be best described as a slightly distorted pentagonal bipyramidal geometry. The nitrosohydroxylaminato groups of the cupferronato anions are essentially planar, while the phenyl ring is nearly coplanar with the plane of the N(O)NO group, in spite of some variation in torsion angles of O(2)–N(2)–C(3)–C(8) and O(4)–N(4)–C(9)–C(10). In the structure of **1**, each half of molecule contains two $SnO_2N_2$ units as five-membered chelate rings (**A** and **B** (Fig. 2)) with O–Sn(1)–O bite angles of 67.95(5)° (**A**) and 66.92(5)° (**B**). The four Sn–O bond lengths around the Sn(1) are not equal. The lengths of the two Sn–O bond in five-membered chelate ring **A** are nearly equal (Δ = 0.003 Å), while those in five-membered chelate ring **B** are slightly different (Δ = 0.048 Å). The Sn–O bond lengths are similar to such bond lengths found in other diorganotin(IV) cupferronato complexes [27]. The Sn–N bond length of 2.415(18) Å is slightly longer than the 2.402(2) Å observed in the polymeric [$Me_2SnCl_2$(4,4′-bipy)]$_n$ complex [28]. All Sn–C bond lengths in the title compound almost are identical, and they are in the typical range of such bonds lengths found in diorganotin(IV) complexes.

Complex **2** crystallized in the triclinic system in the space group of $P\bar{1}$. As can be seen in Fig. 3, crystal structure of **2** is similar to that of **1**. Although there are many main and transition metal

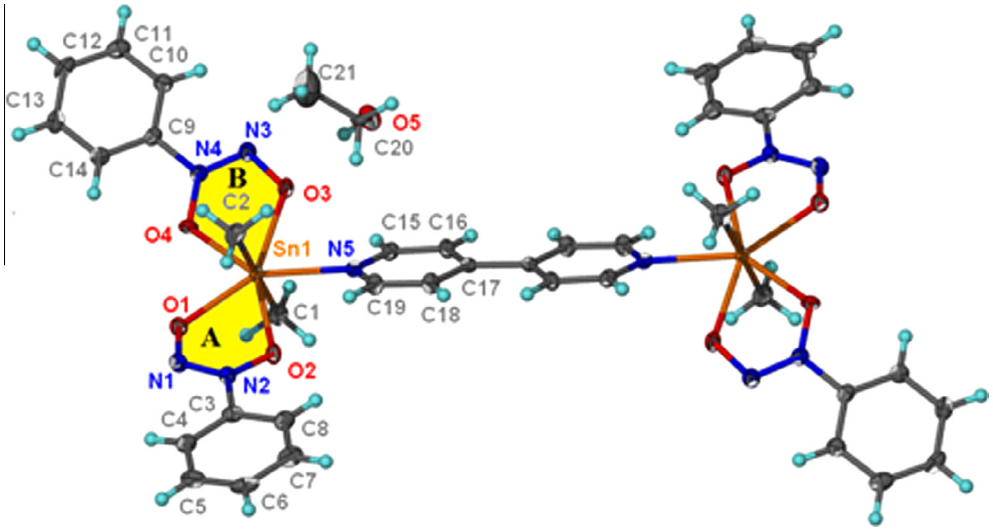


**Fig. 2.** Molecular structure of **1**. Thermal ellipsoids are drawn at 40% probability.

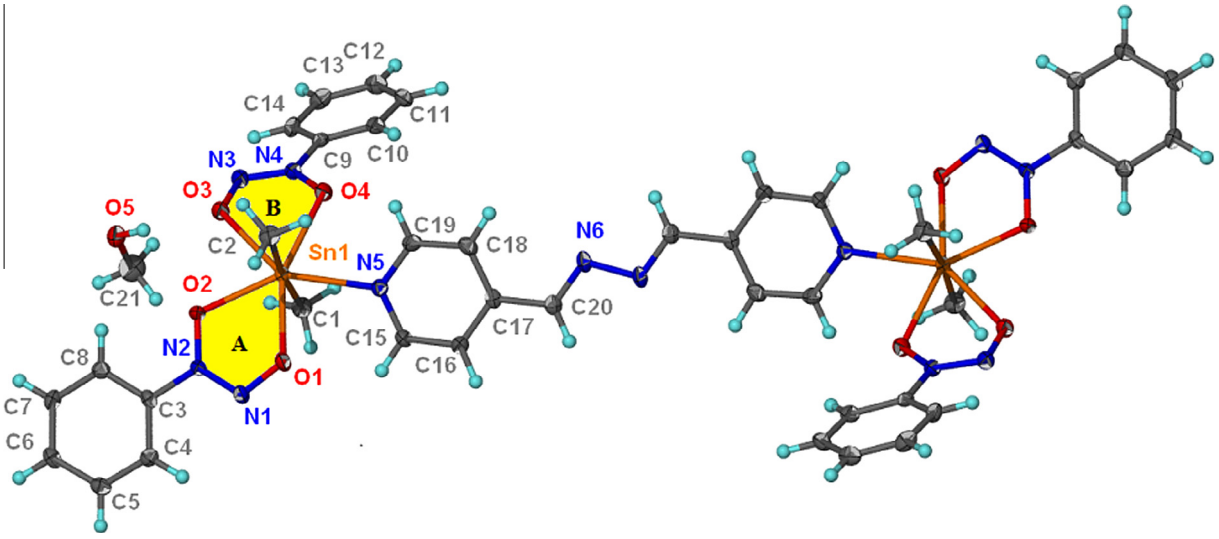


**Fig. 3.** Molecular structure of **2**. Thermal ellipsoids are drawn at 40% probability.

complexes of bipyridil ligand [29–34], to the best of our knowledge, **2** is the first organotin complex with 1,4-bis(4-pyridyl)-2,3-diaza-1,3-butadiene ligand. The structural similarity between **1** and **2** is reflected by the practically unaltered O(1*L*)–Sn(1)–O(2*L*) bite angles [68.40(2)° for **A** and 65.46(5)° for **B**] and differential Sn–O distances (Δ = 0.026 Å for **A**, Δ = 0.038 Å for **B**).

The main factor that controls the packing in structures is the presence of weak intra- and intermolecular interactions. The hydrogen bonding between the C–H and oxygen and nitrogen atoms (Tables S1 and S2, ESI), weak face-to-face π–π stacking interactions (Fig. S2, ESI) between pyridine rings of dipyridil ligands and phenyl rings of cupferronato anion of two adjacent molecules of **1** and **2** with centroid–centroid distance of 3.97 and 3.70 Å and C– interactions (C–H···Cg distance of 2.82 and 2.75 Å) caused more growth of the structures to a 2D supramolecular network.

### 3.4. Thermal behavior

Thermal analysis (TGA-DTA) was employed to study the behavior of **1** and **2** during heat treatment. As thermograms of the complexes illustrate (Fig. S3, ESI), **1** and **2** are stable up to ca. 120 and 175 °C, respectively. The first mass loss between 80 and 90 °C in the TGA curve of both complexes, which is accompanied with an endothermic peak in their DTA curve, is associated with the loss of lattice-solvent molecules. The second endothermic peak in the DTA curves of **1** and **2** at 135 and 180 °C, respectively, without mass loss in their TGA curves is associated with the melting of complexes. Finally, the distinct mass loss from 270 to 360 °C for **1** and 360 to 500 °C for **2**, with a broad exothermic peak in the same temperature range in their DTA curves, is attributed to the elimination of ligands. The solid residue formed at 500 °C is probably $SnO_2$. This investigation shows that the prepared complexes have good thermal stability. Furthermore, it is interesting to note that these complexes are soluble in many solvents, including $CHCl_3$ and MeOH. Therefore, the thin films of these complexes can be prepared readily by spin coating in addition to vacuum deposition. These properties make them potentially good green and yellow-orange emitters in OLEDs.

### 3.5. Optical properties

(Fig. 4) shows the absorption spectra of the prepared complexes and bare ligands in dichloromethane solution. The UV–Vis spectra

**Table 1**
Crystal data and refinement details for **1** and **2**.

| Complex | **1** | **2** |
|---|---|---|
| Molecular formula | $C_{40}H_{46}N_{10}O_9Sn_2$ | $C_{42}H_{50}N_{12}O_{10}Sn_2$ |
| Formula weight | 1048.29 | 1120.32 |
| Crystal dimensions (mm) | 0.25 × 0.25 × 0.25 | 0.30 × 0.25 × 0.20 |
| Crystal color | yellow | yellow |
| Crystal system | monoclinic | triclinic |
| Space group | $P2_1/n$ | $P\bar{1}$ |
| $a$ (Å) | 11.2083(3) | 9.4894(2) |
| $b$ (Å) | 11.5885(3) | 10.9004(4) |
| c (Å) | 16.3461(4) | 12.8940(5) |
| $\alpha$ (°) | | 67.664(4) |
| $\beta$ (°) | 90.113(2) | 75.771(3) |
| $\gamma$ (°) | | 69.785(3) |
| $V$ (Å$^3$) | 2123.15(9) | 1147.56(8) |
| Z | 2 | 1 |
| $F$ (000) | 1056 | 566 |
| Limiting indices | $-13 \leqslant h \leqslant 14$, $-11 \leqslant k \leqslant 15$, $-20 \leqslant l \leqslant 21$ | $12 \leqslant h \leqslant 12$, $-14 \leqslant k \leqslant 14$, $-16 \leqslant l \leqslant 16$ |
| Unique reflections | 4335 | 4882 |
| Calculated density (g cm$^{-3}$) | 1.64 | 1.621 |
| Absorption coefficient (mm$^{-1}$) | 1.243 | 1.158 |
| $\theta$ Range (°) | 2.2–27.6 | 2.31–27.56 |
| Goodness of fit (GOF) on $F^2$ | 1.132 | 1.042 |
| Data/restraints/parameters | 1/18/292 | 1/0/305 |
| Final R indices [$I > 2\sigma(I)$] | $R_1 = 0.0253$, $wR_2 = 0.0709$ | $R_1 = 0.0237$, $wR_2 = 0.0501$ |

**Table 2**
Selected bond distances and angles for **1**.

| Bond lengths (Å) | | Bond angles (°) | |
|---|---|---|---|
| Sn(1)–C(1) | 2.117(3) | C(1)–Sn(1)–C(2) | 179.27(9) |
| Sn(1)–C(2) | 2.118(3) | C(1)–Sn(1)–O(2) | 89.67(8) |
| Sn(1)–O(1) | 2.2698(15) | C(2)–Sn(1)–O(2) | 89.88(8) |
| Sn(1)–O(2) | 2.2668(15) | C(1)–Sn(1)–O(1) | 92.17(7) |
| Sn(1)–N(5) | 2.4152(18) | C(2)–Sn(1)–O(1) | 88.20(8) |
| Sn(1)–O(3) | 2.3284(17) | O(2)–Sn(1)–O(2) | 67.95(5) |

**Table 3**
Selected bond distances and angles for **2**.

| Bond lengths (Å) | | Bond angles (°) | |
|---|---|---|---|
| Sn(1)–C(1) | 2.125(2) | C(1)–Sn(1)–C(2) | 173.93(8) |
| Sn(1)–C(2) | 2.112(2) | C(1)–Sn(1)–O(2) | 91.82(7) |
| Sn(1)–O(1) | 2.2628(13) | C(2)–Sn(1)–O(2) | 94.07(7) |
| Sn(1)–O(2) | 2.2362(14) | C(1)–Sn(1)–O(1) | 89.44(7) |
| Sn(1)–N(5) | 2.4517(16) | C(2)–Sn(1)–O(1) | 94.11(7) |
| Sn(1)–O(3) | 2.3075(13) | O(2)–Sn(1)–O(1) | 68.40(5) |

of 4,4′-bipy, 4-bpdb, and cupferron ligands exhibit bands at 273, 282, and 292 nm, respectively. The absorbency maximums of **1** and **2** are at 302 and 334 nm. The observed bands in the UV–Vis spectra of ligands and complexes can be assigned to $\pi \rightarrow \pi^*$ transitions of the aromatic rings [35–38]. Interestingly, the absorption bands of ligands after coordination to tin red shifted, owing to the formation of the rigid conjugated systems [39]. This confirms that the UV spectra of the complexes are essentially reflections of the absorption of the ligand. The reason for these changes can be explained by the overlap of the absorption spectra region of the ligands. This resulted in a red shift of the major $\pi \rightarrow \pi^*$ electronic transition, indicating that the energy of the $\pi^*$ orbitals increased after the coordination of the nitrogen atom of bipyridyl ligands to the tin atom.

The photoluminescence properties of both complexes and bare ligands and the effect of the π-conjugation length of bipyridyl ligands on photophysical properties of complexes have been investigated. Fig. 5 shows the photoluminescence spectra of the prepared complexes and bare ligands in dichloromethane solution. The emission spectra of 4,4′-bipy, 4-bpdb, and cupferron ligands

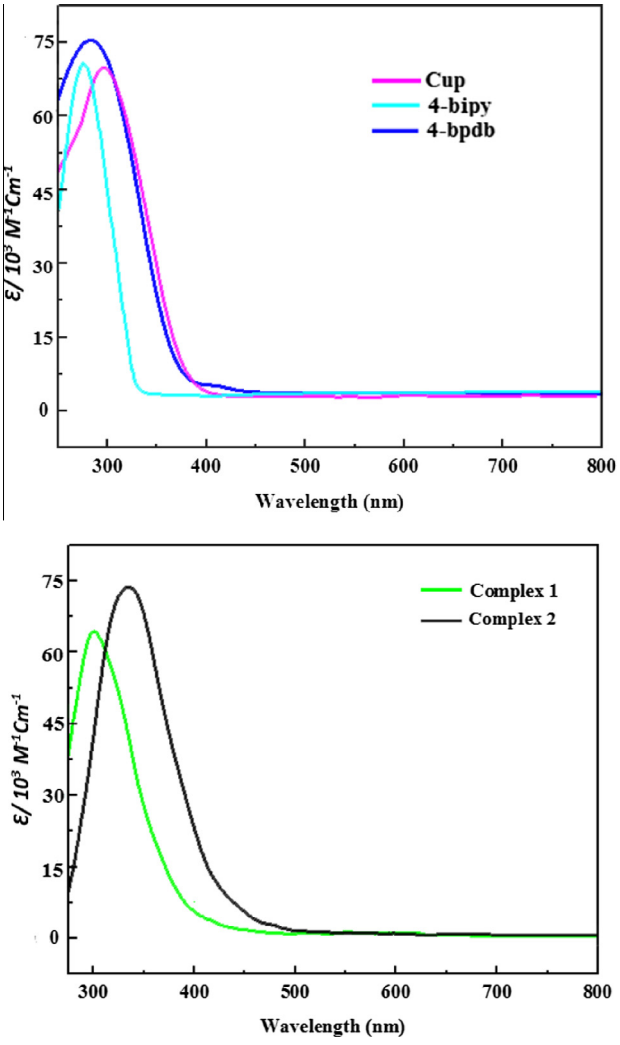


**Fig. 4.** Absorption spectra of **1**, **2** and bare ligands in $CH_2Cl_2$ solution ($10^{-5}$ mol lit$^{-1}$).

exhibit bands at 492, 528, and 537 nm, respectively. The emission spectra of the complexes were collected from 430 to 800 nm with excitation by 100 mW laser at 405 nm. Quantum yields of 0.27 and 0.32 were determined for **1** and **2**, respectively, using quinine sulfate as the standard in all measurements. The quantum yield of complex **2** with a longer π-conjugation length is higher than that of complex **1** with a shorter π-conjugation length. According to the quantum yields and fluorescence spectra of the prepared complexes, both complexes have relatively good fluorescence properties. As expected, based on the PL characterization, fluorescence emissions are observed at the longer wavelengths with red chromaticity rather than at the absorption spectra. The maximum emission wavelengths in $CH_2Cl_2$ solution at room temperature for **1** and **2** are 500 and 548 nm, respectively, and they show that a good correlation exists between the π-conjugation length of bipyridyl ligands and emission wavelengths. As can be seen in Fig. 5, the utilization of 4-bpdb instead of 4,4′-bipy in the structure of **1** enhances the luminescence. In addition, both absorption and emission peaks of **2** are found to be significantly red shifted in comparison with those of **1**. These results can be explained in terms of the decreasing HOMO–LUMO energy gap and the extension of delocalization of the π-electron system along the backbone. In comparison to the absorption maximum of **1**, the absorption maximum of **2** is about 32 nm red shifted. This indicates that the π-electrons are delocalized over the entire conjugated backbone. The photoluminescence spectrum of **2** exhibited a strong emission in the green region with the emission maximum being gradually red shifted with respect to an increase of the π-conjugation length of the fluorescent cores as observed in the absorption spectra.

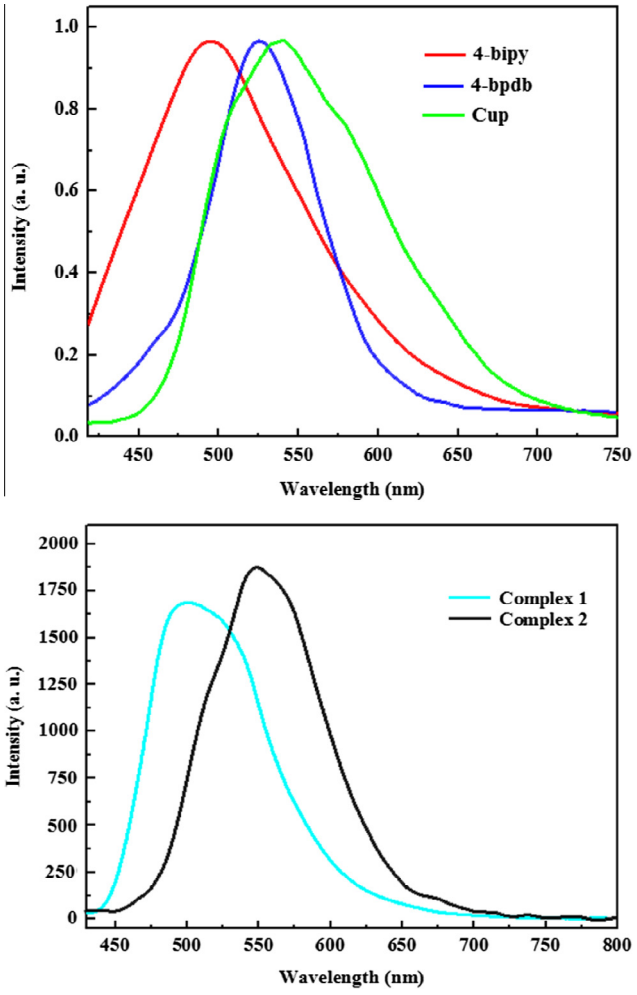


**Fig. 5.** The photoluminescence spectra of **1** and **2** and bare ligands in $CH_2Cl_2$ solution ($10^{-5}$ mol lit$^{-1}$).

### 3.6. Energy levels of prepared complexes

A photoemission apparatus was used for determination of the ionization potential of tin complexes. A thin film of complexes takes over a range of energies using a monochromatic light source. The photocurrent produced from the samples at each energy level was measured. The ionization potential is found by extrapolating the photocurrent until it intercepts the energy axis (Table 4). The electron affinity of tin complexes was appraised by subtracting the energy gap from the ionization potential, where the energy gap was determined by the absorption edge of the UV absorption spectrum of the tin compounds [40,41]. The energy level data for the tin complexes are shown in Table 4.

### 3.7. Electroluminescence characteristic

In order to study the effect of the prepared complexes on the electroluminescence (EL) properties of the organic light-emitting diodes (OLEDs) and to demonstrate their potential application in OLEDs, the prepared complexes were used to fabricate OLED devices with a general configuration of ITO/PEDOT:PSS(90 nm)/PVK:PBD:tin-complex (80 nm)/Al(200 nm). Fig. 6 shows the normalized electroluminescence spectra of the tin complexes. An emissive layer without a tin complex was fabricated to record the EL spectrum of PVK:PBD and to find a relation between the EL spectra of the tin complex and PVK:PBD EL in order to separate it from the emission of the tin complex. The EL spectrum of the PVK:PBD-based device showed a broad peak in the blue region, and the EL of the **1-** and **2-**based devices showed a peak in the green and yellow-orange regions, respectively. The emission characteristics of the devices depended strongly on the structure of the tin complexes' dopants. The EL spectral peak shifted from the high-wavelength region to the low-wavelength region when the bridged ligand changed from 4-bpdb to 4-bipy. This tendency is similar to that of the PL spectra of the corresponding tin complexes. In the EL spectra, the tin complexes showed a long red shift rather than PVK:PBD EL spectra, demonstrating that effective energy transfer was taking place in the emissive layer. As driving voltage was biased to electrodes, the electrons and holes began to inject into the bulk. Some of the electrons and holes under the electric forces formed excitons, which emitted light with their annulation between the HOMO and LUMO energy levels of the layers. The formation of excimers is possible in PVK molecules, since there is an overlap between its absorption and emission spectra. This overlap caused the reduction of EL, which affected the hosting property of the PVK. The effect of excimer formation is decreased when PBD was added to PVK. To achieve a good balance of holes and electrons, both holes and electron-transporting functions should be incorporated into a single bipolar host material [42]. It should be noted that the high ratio of PBD led to lower stability of the device due to the decrease in the ratio of PVK. The ratio of PVK:PBD = 100:40 is suggested as an efficient ratio [43,44], which reduces the risk of excimer formation and increases the stability of the device. The use of a PEDOT:PSS interlayer also helped to establish a better hole injection into the emissive layers, and this resulted in an increase of current and in the probability of exciton

**Table 4**
Energy level for the tin complexes.

| Complex | $E_a$ (eV) | $I_P$ (eV) | $E_g$ (eV) |
|---|---|---|---|
| **1** | 3.14 | 6.3 | 3.16 |
| **2** | 3.13 | 6.0 | 2.87 |

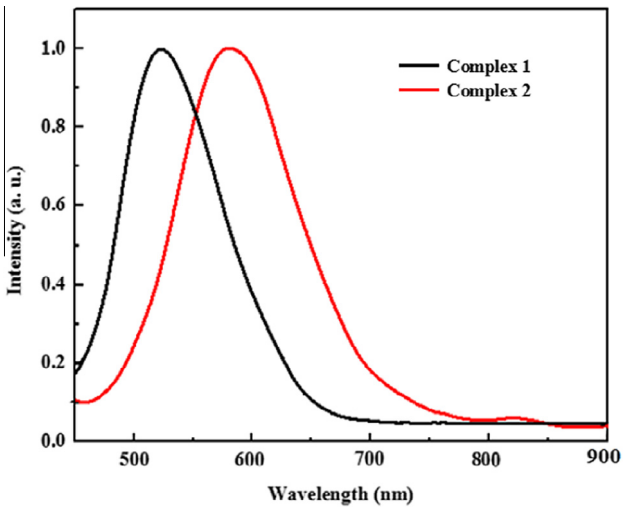


**Fig. 6.** The electroluminescence spectra of **1** and **2**.

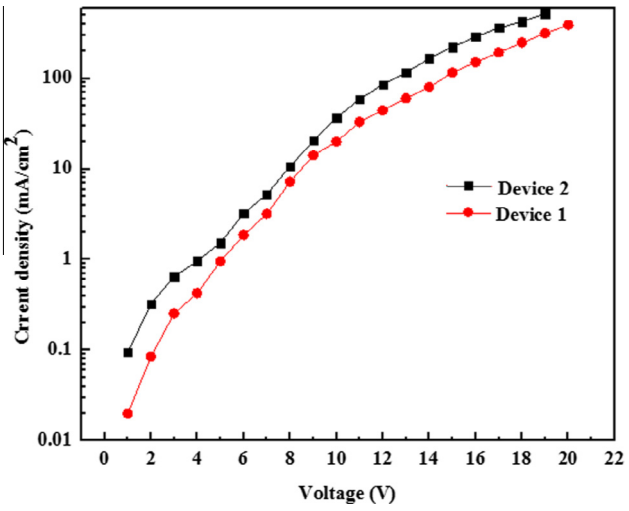


**Fig. 8.** Current density versus applied voltage for **1** and **2** based devices.

formation. Complexes **1-** and **2-**doped PVK:PBD showed emissions at 525 and 578 nm with FWHM (full width at half maximum) of 12.1 and 10.2 eV, respectively. The EL spectra resembles the PL spectra of complexes, indicating that emission comes from the tetravalent tin complex singlet excited states, which formed by the recombination of injected electrons and holes. This can be explained from the energy level diagram of the multi-layer devices (Fig. 7). The energy level of HOMO of PVK and tin complexes is about 5.5 and 6.3 eV and the energy level of LUMO of PVK and tin complexes is about 2.0 and 3.14 eV, respectively. As Fig. 7 shows, in the energy level diagram of the devices, the HOMO and LUMO levels of the tin complexes are located in the PVK:PBD range. This indicates that the injected holes and electrons can directly recombine on the dopant molecules. The injected holes and electrons can directly recombine on the tin complexes' molecules and produce green and yellow-orange lights due to the suitable energy level of the PVK:PBD host and the tin complexes' dopant molecules.

Electrons from the Al are injected into the LUMO level of the PBD as an electron transport layer and then into the LUMO level of the tin complexes, while holes from the ITO are injected into the HOMO level of the PEDOT:PSS and the PVK as the hole-injection and hole transport layer, respectively, and then into the HOMO level of the tin complexes. Finally, electron–hole recombination occurs in the molecules of the tin complexes. As a result, the green and yellow–orange electroluminescence bands are observable. Apparently, an appropriate energy level of PVK:PBD ensures better charge injection for both hole and electron injection into the emission layer. Therefore, more holes and electrons can recombine in the emission layer, and more excitons can form in this layer. Due to the efficient energy transfer from host to dopant, more emissions from the tin complexes can be obtained.

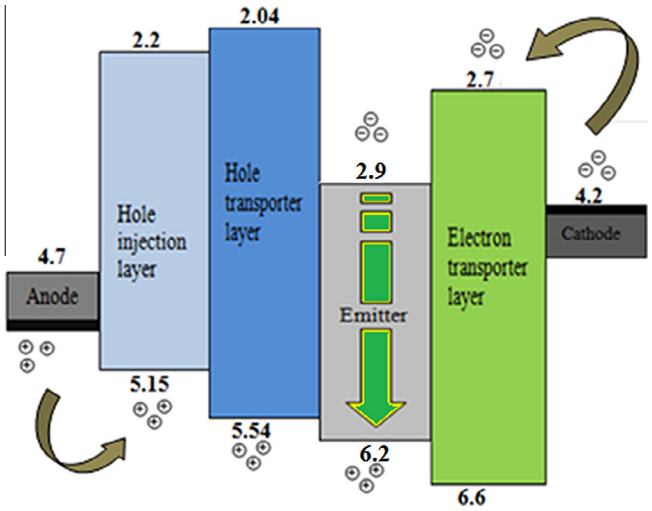


**Fig. 7.** Schematically energy diagram shows the various barriers for charge injection in devices.

The electrical characteristics of the tin complexes into PVK:PBD are shown in Fig. 8. By applying voltage, the electron–hole was injected into the layers, and current density increased. At an applied voltage of 11 V, the current density of **2** was higher than **1**. Apparently, **1** required a larger driving voltage than **2**, indicating that the electron injection barrier increased. This induced the space charge and prevented further injections of carriers from electrodes to bulk [45]. The high operating voltage of **1** will shorten the device lifetime due to thermal aging and impurity diffusion under a high electric field [46].

Fig. 9 shows the luminescence–voltage characteristics of the devices. The maximum brightness of emission levels are 900 and 1098 cd/m$^2$ for **1-** and **2-**based devices, respectively. The device performance is dependent on the π-conjugation length of bipyridyl ligands in tin complexes. The turn-on voltage, defined as the bias voltage at L = 1 cd/m$^2$, changed with the change of π-conjugation length of bipyridyl ligands. It was lower for complex **2** with the long conjugate ligand and higher for complex **1** with the short conjugate ligand. Importantly, the maximum brightness of the devices with different tin complex dopants showed a similar structure effect to the photoluminescence of tin complexes; brighter for the device with tin complex possessing the long conjugate ligand, and less bright for the device with tin complex possessing the short conjugate ligand. These results may provide grounds to consider new tin complexes as promising materials for the design of efficient OLEDs. Finally, the prepared complexes showed good thermal stability according to their melting point measurements and thermal analysis, and they also are stable upon exposure to moisture and air. Therefore, a good level of luminance can be sustained with these complexes.

### *3.8. The effect of doping concentration on the EL properties of the devices*

In order to understand the effect of the doping concentration on the EL properties of the OLEDs, **2** with concentrations of 10% and

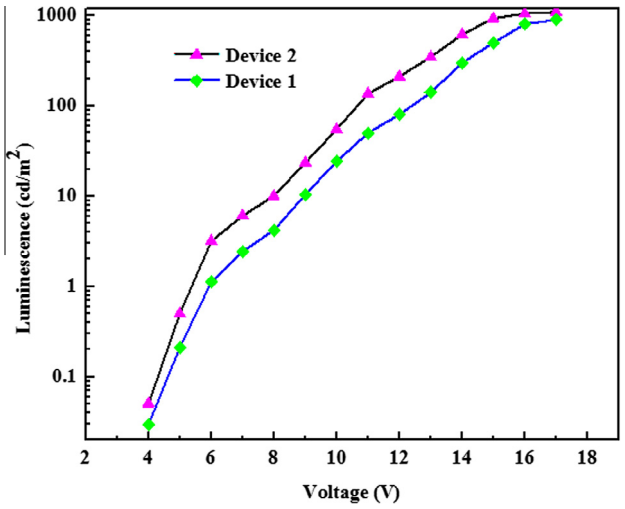


**Fig. 9.** Luminescence–voltage characteristic of **1** and **2** based devices.

20% (w/w) was used as a dopant to fabricate two OLED devices, and their electroluminescence properties were investigated. The EL spectra of the devices with 10% and 20% (w/w) of **2** as the dopant showed a yellow-orange emission at 578 and 589 nm with FWHM (full width at half maximum) of 10.2 and 10.7 eV, respectively. As can be seen in Fig. 10, the height concentration of the dopant generally caused a trap effect in the current voltage and led to the self-quenching of emission and a reduction in the efficiency of the device. Fig. S4 shows the current density versus the voltage of the two OLEDs. Apparently, there is an inverse relationship between the complex concentration and the current density change at a specific voltage. Notably, the increase of complex concentration resulted in an increase of in surface roughness and a decrease in carrier transport and device efficiency. The device with 10% of **2** had a much lower operation voltage than that of the device with 20% of **2**. This suggests improved electron injection, and the result is in accordance with an increase in the number of exciton recombination mechanisms. As Fig. S5 illustrates, the maximum brightness of the devices with 10% and 20% (w/w) of **2** are 1098 and 940 cd/m$^2$, respectively. It can be seen that the luminance of the OLEDs decreases with the increase in the doping concentration of **2** at the same voltage. This can be understood by considering the effects of concentration quenching and trapping of dopant molecules.

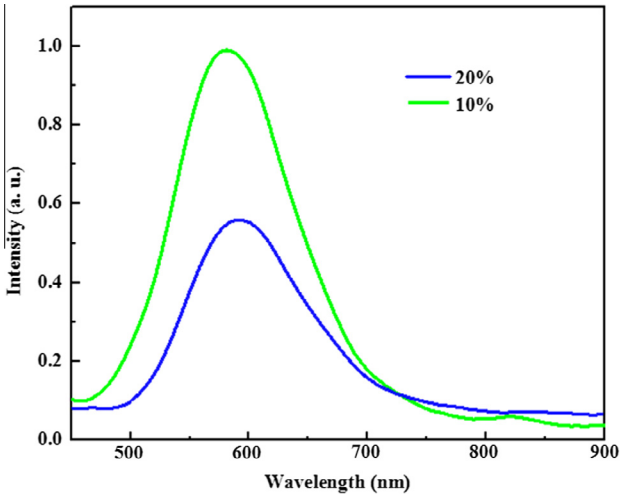


**Fig. 10.** The EL spectra of the devices with 10 and 20% (w/w) of **2** as the dopant.

Fig. S6 shows atomic force microscope (AFM) images of the premixed of PVK:PBD:complex **2** with a scanning area of 5 × 5 μm. The average root-mean-square (RMS) surface morphologies of the films with 10% and 20% (w/w) of **2** as the dopant were about 8.2 and 11.2 nm, respectively. This showed that the surface roughness of the layer with a concentration of 20% was certainly larger than the layer with a concentration of 10%. As a result, more effective electron injection should be achieved at a layer with 10% concentration because of the increased contact area between the electron transport layer (ETL) and the cathode.

## 4. Conclusions

Two new organotin(IV) complexes have been synthesized and characterized by spectroscopic methods in addition to their single-crystal structures. The intensity of the fluorescence band of **2** containing the long conjugated rigid ligand is higher than the band of **1**. In addition, both absorption and emission peaks of **2** are found to be significantly red shifted in comparison with those of **1**. The results showed that the π-conjugation length of ligand is an effective parameter in tuning of the emission wavelength. The EL spectra of tin complexes illustrated a broad red shift rather than a PVK:PBD blend. It has been demonstrated that the concentration of the prepared complex changes the driving voltage and also the shift of the I-V diagram to high voltage by increasing the complex concentration. The prepared complexes showed fluorescence emissions at room temperature in solution and have good stability in air and in a high-temperature environment, which make them suitable for the fabrication of OLEDs. Finally, all properties and features suggest that this novel tin(IV) complex is a good candidate as an emitting layer material in OLEDs and other devices.

## Acknowledgment

The authors thank the Vice-President's Office for Research Affairs of Shahid Beheshti University for supporting this work.

## Appendix A. Supplementary material

CCDC 904685 and 928776 contains the supplementary crystallographic data for **1** and **2**. These data can be obtained free of charge from The Cambridge Crystallographic Data Centre via www.ccdc.cam.ac.uk/data_request/cif. Supplementary data associated with this article can be found, in the online version, at http://dx.doi.org/10.1016/j.ica.2014.02.032.

## References

[1] C.W. Tang, S.A. Van Slyke, Appl. Phys. Lett. 51 (1987) 913.
[2] C.W. Tang, S.A. Van Slyke, C.H. Chen, J. Appl. Phys. 65 (1989) 3610.
[3] J. Kido, K. Nagai, Y. Okamoto, T. Skotheim, Appl. Phys. Lett. 59 (1991) 2760.
[4] C. Adachi, S. Tokito, T. Tsutsui, S. Saito, Jpn. J. Appl. Phys. 27 (1988) L713.
[5] J.H. Burroughes, D.D.C. Bradley, A.R. Brown, Nature 347 (1990) 539.
[6] P.F. Wang, Z.R. Hong, Z.Y. Xie, S.W. Tong, O. Wong, C.S. Lee, N.B. Wong, L.S. Hung, S.T. Lee, Chem. Commun. (2003) 1664.
[7] G. Yu, Y.Q. Liu, Y.R. Song, X. Wu, D.B. Zhu, Synth. Met. 117 (2001) 211.
[8] T. Yu, W. Su, W. Li, Z. Hong, R. Hua, M. Li, B. Chu, B. Li, Z. Zhang, Z.Z. Hu, Inorg. Chim. Acta 359 (2006) 2246.
[9] A. Majumder, V. Gramlich, G.M. Rosair, S.R. Batten, J.D. Masuda, M.S. El Fallah, O.J. Ribas, O.P. Sutter, C.D. Desplanches, S. Mitra, Crysth. Growth. Des. 6 (2006) 2355.
[10] M. Brinkmann, B. Fite, S. Pratontep, C. Chaumont, Chem. Mater. 16 (2004) 4627.
[11] P.E. Burrows, L.S. Sapochak, D.M. McCarty, S.R. Forrest, M.E. Thompson, Appl. Phys. Lett. 64 (1994) 2718.
[12] P.E. Burrows, Z. Shen, V. Bulovic, D.M. McCarty, S.R. Forrest, J.A. Cronin, M.E. Thompson, J. Appl. Phys. 79 (1996) 7991.
[13] L.S. Sapochak, F.E. Benincasa, R.S. Schofield, J.L. Baker, K.K. Riccio, D. Fogarty, H. Kohlmann, K.F. Ferris, P.E. Burrows, J. Am. Chem. Soc. 124 (2002) 6119.
[14] H.B. Michaelson, J. Appl. Phys. 48 (1977) 4729.

[15] X.T. Tao, M. Shimomura, H. Suzuki, S. Miyata, H. Sasabe, Appl. Phys. Lett. 76 (2000) 3522.
[16] A. Patra, P. Michael, S. Christopher, Chem. Mater. 14 (2002) 4044.
[17] H.C. Yeh, S.J. Yeh, C.T. Chen, Chem. Commun. (2003) 2632.
[18] L.S. Sapochak, A. Padmaperuma, N. Washton, J. Am. Chem. Soc. 123 (2001) 6300.
[19] Y.T. Tao, E. Balasubrmaniam, A. Danel, B. Jarosz, P. Tomasik, Chem. Mater. 13 (2001) 1207.
[20] D.M. Ciurtin, Y.B. Dong, M.D. Smith, T. Barclay, Inorg. Chem. 40 (2001) 2825.
[21] D.D. Perrin, W.L.F. Armarego, D.R. Perrin, Purification of Laboratory Chemicals, Pergamon Press, 2nd Ed., 1980, 20.
[22] SMART, APEX2, version 2.1. Madison, WI: Bruker AXS Inc., 2005.
[23] G.M. Sheldrich, SADABS, University of Gottingen, Germany, 2005.
[24] G.M. Sheldrich, SHELXS-97, University of Gottingen, Germany, 1997.
[25] APEX2 and SAINT, Bruker AXS Inc, Madison, Wisconsin, USA, 2008.
[26] T.S. Baul, W. Rynjah, X. Song, G. Eng, A. Linden, J. Organomet. Chem. 692 (2007) 3392.
[27] A. Szorcsik, L. Nagy, I. Kokeny, A. Deak, M. Scopelliti, T. Fiore, L. Pellerito, J. Organomet. Chem. 692 (2007) 3409.
[28] C. Ma, J. Zhang, R. Zhang, Heteroatom Chem. 14 (2004) 338.
[29] M. Cattaneo, F. Fagalde, E.N. Katz, Inorg. Chem. 45 (2006) 127.
[30] A.E. Dennis, M.H. Grace, F.M. Mary, C.M. Kieran, R.G.R. Guy, Polyhedron 17 (1998) 2321.
[31] Y.B. Dong, J.Y. Cheng, J.P. Ma, H.Y. Wang, R.Q. Huang, D.S. Guo, M.D. Smith, Solid State Sci. 5 (2003) 1177.
[32] Y.B. Dong, M.D. Smith, R.C. Layland, Inorg. Chem. 39 (2000) 4927.
[33] Y.B. Dong, J.P. Ma, R.Q. Huang, F.Z. Liang, M.D. Smith, Dalton Trans. (2003) 1472.
[34] Y.B. Dong, L. Wang, J.P. Ma, D.Y. Zhao, D.Y. Shen, R. Huang, Cryst. Growth Des. 6 (2006) 2475.
[35] R.S. Addleman, M. Carrott, C.M. Wai, T.E. Carleson, B.W. Wenclawiak, Anal. Chem. (2001) 1112.
[36] J. Huang, X. Wang, A.J. Jacobson, J. Mater. Chem. 13 (2003) 191.
[37] V.A. Volkovich, T.R. Griffiths, D.J. Fray, R.C. Thield, Phys. Chem. Chem. Phys. 3 (2001) 5182.
[38] Y.S. Jiang, Z.T. Yu, Z.L. Liao, G.H. Li, J.S. Chen, Polyhedron 25 (2006) 1359.
[39] G.X. Wang, Y.W. Zhang, Inorg. Chim. Acta 376 (2011) 212.
[40] K. Singh, A. Kumar, R. Srivastava, P.S. Kadyan, M.N. Kamalasanan, Opt. Mater. 34 (2011) 221.
[41] R.S. Ashraf, M. Shahid, E. Klemm, M. Al-Ibrahim, S. Sensfuss, Macromol. Macromol. Rapid. Commun. 27 (2006) 145401.
[42] B. Ma, B.J. Kim, L. Deng, D. Poulsen, M.E. Thompson, J. Frechet, Macromolecules 40 (2007) 8156.
[43] J. Yang, K. Gordon, Chem. Phys. Lett. 385 (2004) 481.
[44] S. Chang, C. Fan, C. Lai, Y. Chao, S. Hu, Surf. Coat. Technol. 200 (2006) 3289.
[45] C.C. Lee, M.Y. Chang, P.T. Huang, Y.C. Chen, Y. Chang, S.W. Liu, J. Appl. Phys. 101 (2007) 1145.
[46] N.H. Yusoff, M.M. Salleh, M. Yahaya, Solid State Sci. Technol. 16 (2008) 63.